Available online at www.sciencedirect.com
ScienceDirect
Trans. Nonferrous Met. Soc. China 22(2012) 810−818
Transactions of Nonferrous Metals Society of China
www.tnmsc.cn

Dry sliding wear behavior of AA6061/ZrB_2 in-situ composite

I. DINAHARAN[1], N. MURUGAN[2]

1. Department of Mechanical Engineering, Karunya University, Coimbatore−641 114, Tamil Nadu, India;
2. Department of Mechanical Engineering, Coimbatore Institute of Technology, Coimbatore−641 014, Tamil Nadu, India

Received 6 May 2011; accepted 9 August 2011

Abstract: The dry sliding wear behavior of AA6061/ZrB_2 in-situ composite prepared by the reaction of inorganic salts K_2ZrF_6 and KBF_4 with molten aluminum was investigated. An attempt was made to develop a mathematical model to predict the wear rate of AA6061/(0−10%) ZrB_2 in-situ composites. Four-factor, five-level central composite rotatable design was used to minimize the number of experiments. The factors considered are sliding velocity, sliding distance, normal load and mass fraction of ZrB_2 particles. The effect of these factors on the wear rate of the fabricated composite was analyzed and the predicted trends were discussed by observing the wear surface morphologies. The in-situ formed ZrB_2 particles enhance the wear performance of the composite. The wear rate of the composite bears a proportional relationship with the sliding velocity, sliding distance and normal load.
Key words: aluminum matrix composites; ZrB_2; dry sliding wear; mathematical model

1 Introduction

Aluminum alloys are extensively used in several engineering fields including aerospace, automotive, marine and military [1,2]. However, aluminum alloys exhibit poor tribological properties. The incorporation of hard ceramic particles into aluminum alloys helps to improve the mechanical and tribological properties. The resulting material is universally known as aluminum matrix composites (AMCs). The superior properties of AMCs such as high wear resistance, low thermal expansion, and high specific strength have created an interest for feasible replacement of aluminum alloys in many products and applications [3,4].

The properties of the AMCs depend on the type, size, shape, mass or volume fraction and spatial distribution of ceramic particles in the aluminum matrix [5]. The bonding and nature of interface existing between the ceramic particle and the aluminum matrix plays a crucial role in dictating the properties [6]. The fabrication method influences the bonding strength to a larger extent [7].

AMCs are currently prepared by a number of methods including powder metallurgy, mechanical alloying, squeeze casting, compo casting, stir casting etc [8,9]. Liquid method of processing is effective owing to its simplicity, ease of adoption, and applicability to large quantity fabrication. Liquid method of processing involves either adding ceramic particles externally to the molten metal or synthesizing in the melt itself. The former is known as stir casting while the later is called as in-situ fabrication. In-situ fabrication involves chemical reaction of inorganic salts or metallic powders with the molten metal and ceramic particles are formed inside the melt. The surface of the particles produced in the in-situ process tends to be free of contamination, which improves the interfacial bonding strength. Uniform distribution of the fine size particles is effortlessly achieved without the need for the addition of wetting agent [10].

Among feasible ceramic reinforcements, ZrB_2 possesses strong covalent bonding, high melting point, high strength and hardness, good thermal conductivity and thermal shock resistance, which make it a good promising candidate for extreme environments associated with aerospace industry [11]. Due to the unique properties of ZrB_2, it has the potential to be substituted for Al_2O_3 and SiC [12].

Some studies on the dry sliding wear behavior of

Corresponding author: I. DINAHARAN; Tel: +91-9444107013; E-mail: dinaweld2009@gmail.com
DOI: 10.1016/S1003-6326(11)61249-1

in-situ composites have been reported in the recent years. MANDAL et al [13] studied the effect of TiB_2 particles on the wear resistance of Al−4Cu/(0−10%) TiB_2 in-situ composite and reported an improved wear resistance with increasing the mass fraction of TiB_2. KUMAR et al [14] observed an enhancement in wear resistance of Al−7Si/(0−10%)TiB_2 in-situ composite with the addition of TiB_2. HERBERT et al [15] compared the wear resistance of as cast Al−4.5Cu/5%TiB_2 in-situ composite with mushy state rolled composite and reported an improvement in wear resistance subsequent to rolling. ZHANG et al [16] analyzed the wear rate of A356/(0−25%)(Al_3Zr+ZrB_2) in-situ composite and recorded an enhancement in wear resistance with increased mass fraction of Al_3Zr and ZrB_2 particles. KUMAR et al [17] investigated the effect of ZrB_2 particles and heat treatment on the wear rate of AA6351/(0−9%)ZrB_2 in-situ composite and found a reduction in wear rate with the addition of ZrB_2. Those researchers examined the effect of one or two factors such as mass fraction of ceramic particles and normal load on the dry sliding wear behavior of the in-situ composites.

The present work is an attempt to develop a mathematical model to predict the wear rate of AA6061/(0−10%)ZrB_2 in-situ composite and analyze the influence of sliding velocity (v), sliding distance (D), normal load (F) and mass fraction of ZrB_2 particles (c) on wear rate (W). AA6061 was used as matrix. Experiments were conducted according to central composite rotatable design. A number of researchers utilized central composite rotatable design to conduct experiments and developed precise mathematical models to predict the influence of process parameters on the responses [18−23].

2 Experimental

The AA6061-T6 rods (d25 mm) were melted in an electrical furnace using a graphite crucible. The chemical composition of AA6061 rods is presented in Table 1. The weighed quantities of inorganic salts K_2ZrF_6 and KBF_4 were added into the molten aluminum to produce ZrB_2. The temperature of the melt was maintained at 860 °C. The melt was stirred intermittently for 30 min. After removing slag the melt was poured into a preheated die. Castings were obtained with different mass fractions (0, 2.5%, 5%, 7.5% and 10%) of ZrB_2. The detailed fabrication procedure and formation of in-situ ZrB_2 particles are available elsewhere [16,17,24]. Specimens with dimensions of 25 mm×25 mm×6 mm were prepared from the castings to study the microstructure. The specimens were polished as per standard metallographic practice and etched with a colour etchant containing 2−3 g sodium molybdate, 5 mL HCl (35%) and 1−2 g ammonium bifluoride in 100 mL distilled water [25]. The etched specimens were observed using an optical microscope (OLYMPUS-BX51M).

Table 1 Chemical composition of AA6061-T6 (mass fraction, %)

Mg	Si	Fe	Mn	Cu
0.95	0.54	0.22	0.13	0.17
Cr	Zn	Ni	Ti	Al
0.09	0.08	0.02	0.01	Bal.

The predominant parameters which influence the wear rate of AMCs are sliding velocity, sliding distance, normal load and mass fraction of ZrB_2 particles [5]. The decided levels of those selected parameters based on trial experiments along with their units and notations are given in Table 2. The lower limit of each parameter was chosen to yield a noticeable wear. The upper limit of each parameter was fixed without causing severe wear. The upper limit of a parameter was coded as 2 and the lower limit was coded as –2 for the convenience of recording and processing experimental data. The coded values for intermediate values are calculated using the following relationship.

$$X_i=2[2X-(X_{max}+X_{min})]/(X_{max}-X_{min}) \quad (1)$$

where X_i is the required coded value of a variable X; X is any value of the variable from X_{min} to X_{max}; X_{min} is the lowest level of the variable; X_{max} is the highest level of the variable.

Table 2 Sliding wear parameters and their levels

Parameter	Notation	Unit	Level				
			−2	−1	0	1	2
Sliding velocity	v	m/s	0.4	0.8	1.2	1.6	2
Sliding distance	D	m	500	1000	1500	2000	2500
Normal load	F	N	5	10	15	20	25
ZrB_2 content	c	%	0	2.5	5	7.5	10

The central composite rotatable factorial design consisting of 31 sets of coded conditions shown in Table 3 was used to carry out the experiments. The detailed description of the design matrix is available elsewhere [26]. Specimens with dimensions of 6 mm×6 mm×25 mm were obtained from the castings. The wear rate was measured using a pin-on-disc wear apparatus (DUCOM TR20-LE) at room temperature according to ASTM G99—05 standard. The polished surface of the pin was slid on a hardened chromium steel disc. A computer-

aided data acquisition system was used to monitor the loss of height. The volumetric loss was computed by multiplying the cross section of the test pin with its loss of height [13]. The experiments were carried out as per design matrix at random to eliminate any systematic errors creeping into the system. The estimated wear rate is recorded in Table 3. The wear surface of selected specimens was observed using scanning electron microscope (JEOL-JSM−6390).

Table 3 Design matrix and estimated wear rate

Trial run	Sliding wear parameter				Wear rate/ (10^{-5} mm^3·m^{-1})
	v	D	F	c	
T01	−1	−1	−1	−1	518
T02	+1	−1	−1	−1	551
T03	−1	+1	−1	−1	531
T04	+1	+1	−1	−1	574
T05	−1	−1	+1	−1	540
T06	+1	−1	+1	−1	580
T07	−1	+1	+1	−1	560
T08	+1	+1	+1	−1	630
T09	−1	−1	−1	+1	320
T10	+1	−1	−1	+1	360
T11	−1	+1	−1	+1	367
T12	+1	+1	−1	+1	383
T13	−1	−1	+1	+1	353
T14	+1	−1	+1	+1	378
T15	−1	+1	+1	+1	387
T16	+1	+1	+1	+1	409
T17	−2	0	0	0	396
T18	+2	0	0	0	533
T19	0	−2	0	0	389
T20	0	+2	0	0	511
T21	0	0	−2	0	403
T22	0	0	+2	0	514
T23	0	0	0	−2	742
T24	0	0	0	+2	295
T25	0	0	0	0	446
T26	0	0	0	0	468
T27	0	0	0	0	451
T28	0	0	0	0	432
T29	0	0	0	0	456
T30	0	0	0	0	463
T31	0	0	0	0	444

3 Development of mathematical model

The wear rate of the fabricated composite is a function of sliding velocity, sliding distance, normal load and mass fraction of ZrB_2, which can be expressed as:

$$W=f(v, D, F, c) \quad (2)$$

The second order polynomial regression equation used to represent the response surface 'Y' for k factors is given by

$$Y = b_0 + \sum_{i=1}^{k} b_i X_i + \sum_{i=1}^{k} b_{ii} X_i^2 + \sum_{i=1}^{k} b_{ij} X_i X_j \quad (3)$$

where b_0 is the average of responses, and b_i, b_{ii} and b_{ij} are the coefficients which depend on the respective main and interaction effects of the parameters. The values of the coefficients were estimated using the following expressions [26]:

$$b_0=0.142857(\sum Y)-0.035714\sum\sum(X_{ii}Y) \quad (4)$$

$$b_i=0.041667\sum(X_iY) \quad (5)$$

$$b_{ii}=0.03125\sum(X_{ii}Y)+0.00372\sum\sum(X_{ii}Y)-0.035714(\sum Y) \quad (6)$$

$$b_{ij}=0.0625\sum(X_{ii}Y) \quad (7)$$

The selected polynomial for four factors could be expressed as:

$$W=b_0+b_1v+b_2D+b_3F+b_4c+b_{11}v^2+b_{22}D^2+b_{33}F^2+b_{44}c^2+ b_{12}vD+b_{13}vF+b_{14}vc+b_{23}DF+b_{24}Dc+b_{34}Fc \quad (8)$$

The coefficients were calculated using the software SYSTAT 12. The mathematical model was developed after determining the coefficients. All the coefficients were tested for their significance at 95% confidence level. The insignificant coefficients were eliminated without affecting the accuracy of the mathematical model using t-test. The significant coefficients were taken into account to construct the final mathematical model. The developed final mathematical model with sliding wear parameters in coded form is given as:

$$W=452.079+23.458v+20.208D+18.958F- 100.875c+15.398c^2 \quad (9)$$

The adequacy of the developed mathematical model was tested using the analysis of variance (ANOVA) technique which is presented in Table 4. The calculated values of F-ratio are greater than the tabulated values at 95% confidence level, which means the developed mathematical model is considered to be adequate [26]. The model has a higher r^2 value of 0.97. Figure 1 shows the scatter diagram of the developed mathematical model. The experimental values and predicted values from the mathematical model are scattered both sides and close to 45° line, which further proves the adequacy of the model.

Table 4 ANOVA results of developed mathematical model

Response	Source	Sum of squares	Degree of freedom	Mean-square	F-ratio (calculated)	F-ratio (tabulated)	P-value
W	Regression	282827.806	5	56565.56	183.032	2.60	0
	Residual	7726.194	25	309.05			

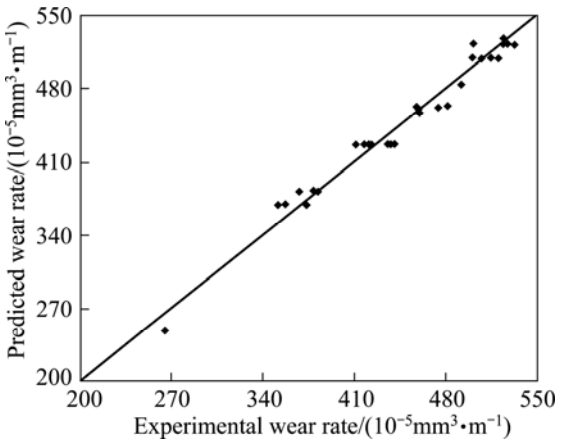

Fig. 1 Scatter diagram of developed model

Experiments were conducted to confirm the validity of the developed mathematical model. Five tests were conducted using different values of sliding velocity, sliding distance and normal load other that those used in the design matrix and their wear rate was estimated. The results obtained are shown in Table 5. The error in prediction is calculated as [(experimental value–mathematical model value)/mathematical model value]× 100. It is found from the table that the error is within ±7%, which confirms the accuracy of the developed mathematical model.

Table 5 Results of conformity experiments

Trial run	Sliding wear parameter				Wear rate/ (10^{-5} mm^3·m^{-1})		Error/ %
	v	*D*	*F*	*c*	Experimental	Predicted	
1	1.25	−1.50	−1	−2	667.80	695.47	−3.98
2	0.75	−0.25	0	−1	620.15	580.89	6.76
3	0.25	−0.75	2	0	505.20	480.70	5.10
4	−0.5	0.75	1	1	405.25	388.99	4.18
5	−1.5	−1.25	−2	2	225.45	213.56	5.57

4 Results and discussions

The effects of wear parameters such as sliding velocity, sliding distance, normal load and mass fraction of ZrB_2 particles on the wear rate of AA6061/ZrB_2 in-situ composite were evaluated using the developed mathematical model. The trends obtained for each wear parameter are represented in graphical form. The possible causes for the effects of different parameters on wear rate are elaborated as follows.

4.1 Effect of ZrB_2 particles

Figure 2 shows the wear rate of AA6061/ZrB_2 in-situ composite as a function of mass fraction of ZrB_2 particles. The figure shows that the wear rate decreases with increasing the mass fraction of ZrB_2 particles with constant wear parameters. The decrease in wear rate is not linear.

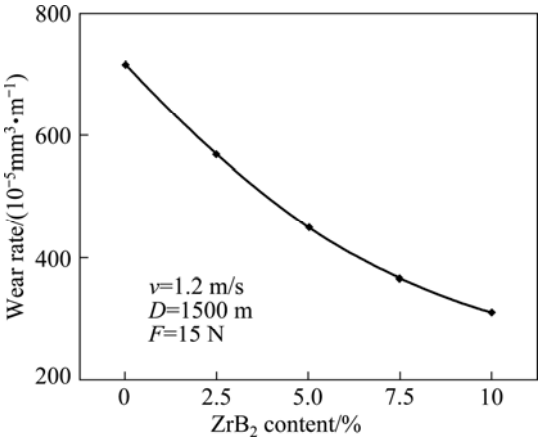

Fig. 2 Effect of mass fraction of ZrB_2 on wear rate

The addition of in-situ formed ZrB_2 particles improves the hardness of matrix alloy, which reduces the rate of material removal. The average thermal expansion coefficient of AA6061 is 24×10^{-6} °C^{-1} while that of ZrB_2 is 6.6×10^{-6} °C^{-1}. This difference in thermal expansion between matrix and reinforcement tends to cause high density of dislocations around ZrB_2 particles during solidification. The interaction between ZrB_2 particles and dislocations enhances the wear resistance.

Figure 3 shows the micrographs of the fabricated composite. The inherent characteristic of in-situ fabrication method is the ability to provide a pure interface [10]. The micrographs demonstrate the existence of a clean interface between the matrix and ZrB_2 particle. Neither voids nor reaction products surround the particle which is well bonded with the matrix alloy. The pure interface increases the load bearing capacity of the composite, which means higher stress is needed initially to cracking. This brings down the wear rate of the composite with increasing the mass fraction of ZrB_2 particles. Further the spherical shape of the particles delays crack initiation.

The nonlinear behavior of the composite can be described as follows. The in-situ reaction of K_2ZrF_6 and KBF_4 with molten aluminum produces ZrB_2 particles at

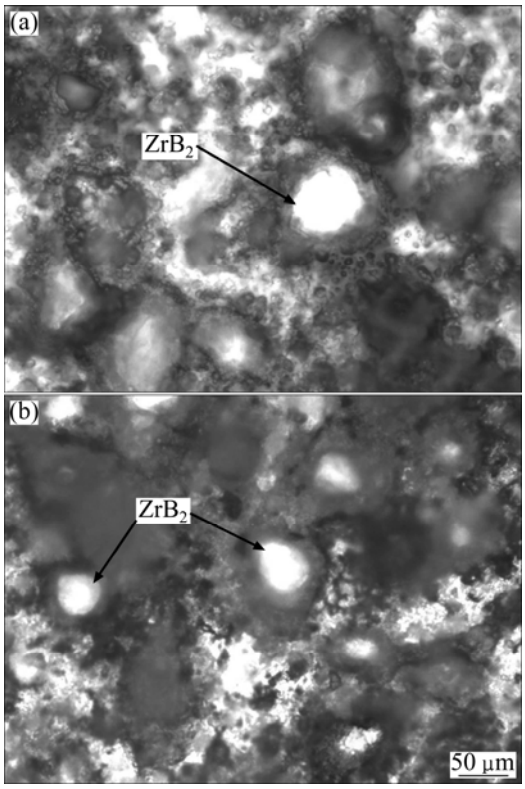

Fig. 3 Micrographs of fabricated composite containing 5% (a) and 7.5% (b) ZrB_2

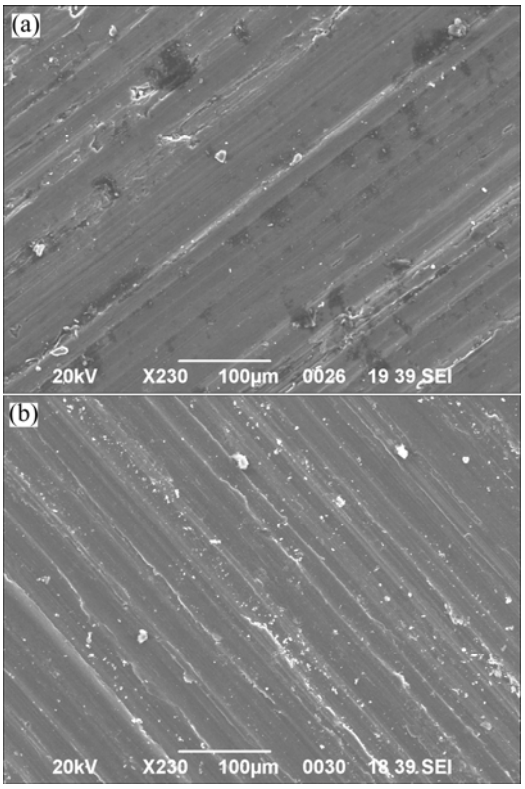

Fig. 4 SEM micrographs of wear surface of fabricated composite containing 0% (T23) (a) and 10% (T24) (b) ZrB_2

varying sizes (1−50 μm). The reaction rate influences the size of particles to a larger extent [17]. The reaction rate is dependent on the amount of inorganic salts added. When more amount of inorganic salts are added to produce higher mass fraction of ZrB_2 particles, the reaction rate increases. The particles tend to coarsen due to the increased reaction rate, which causes complex process of material removal during sliding wear. Therefore, the wear rate of the composite decreases nonlinearly.

Figure 4 reveals the SEM micrographs of the wear surfaces of AA6061 and AA6061/10%ZrB_2. In Fig. 4(a), the wear surface of AA6061 shows the presence of deep grooves, large number of pits and cracks. High plastic deformation is observed at the edges of the grooves. The plastic deformation is caused by the frictional heat which softens the surface. In Fig. 4(b), the wear surface of AA6061/10%ZrB_2 shows shallow grooves and fewer pits. The depth of the grooves is reduced due to the presence of ZrB_2 particles. Lower plastic deformation is observed at the edges of the grooves. The wear debris are loose in nature and not adhering to the surface due to hard ZrB_2 particles. The grooves and ridges are parallel and aligned along the direction of sliding. It is evident from the wear surface that when the content of ZrB_2 particle increases, the wear rate reduces.

4.2 Effect of sliding velocity

Figure 5 shows the effect of sliding velocity on the wear rate of AA6061/ZrB_2 in-situ composite. It is evident from the figure that the wear rate increases linearly with the increase of sliding velocity.

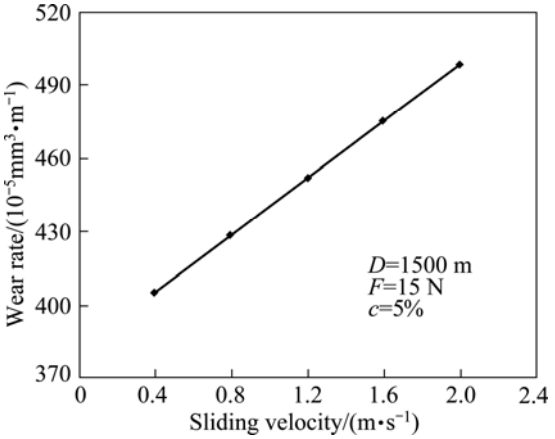

Fig. 5 Effect of sliding velocity on wear rate

The sliding velocity strongly influences the frictional heat generated between the counter surfaces [27]. The frictional heat softens the pin surface. The degree of softening depends on the degree of frictional heat. The penetration of the hard asperities of the counter surface into the pin surface increases with the increased

degree of softening. The pin is subjected to less frictional heat at 0.4 m/s and the penetration of the counter surface is less, which leads to lower wear rate. As the sliding velocity increases, the pin is subjected to higher frictional heat and the penetration of the counter surface becomes more, which leads to higher wear rate. The subsurface experiences higher strain rate with increased sliding velocity. The increased rate of deformation of subsurface increases the wear rate.

The thermal mismatch between the matrix alloy and ZrB_2 particle also plays a role in sliding wear [16]. The thermal mismatch creates an interface stress. When the interface stress exceeds the interface bond strength, cracks will form and particles will be pulled off. The pulled off particles act as wear debris and start third body abrasion. The interface stress increases with increased sliding velocity due to higher frictional heat. Hence, more particles are pulled off, which result in increased wear rate.

Figure 6 depicts the SEM micrographs of the wear surface of the fabricated composite at sliding velocities of 0.4 and 2 m/s. In Fig. 6(a), shallow grooves, patches of damaged regions and delamination of the matrix alloy are seen at the sliding velocity of 0.4 m/s. The deformation of the subsurface is less. In Fig. 6(b), the grooves have become deep and severely damaged regions are seen at a sliding velocity of 2 m/s. The deformation of the subsurface is more. The wear surface has been subjected to higher frictional heat. It is evident from the wear surface that increase in sliding velocity increases the wear rate of the composite.

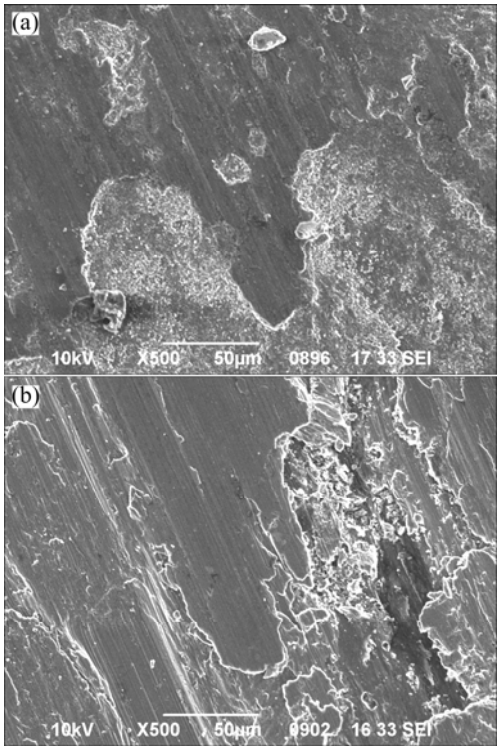

Fig. 6 SEM micrographs of wear surface of fabricated composite tested at sliding velocity of 0.4 m/s (T19) (a) and 2 m/s (T20) (b)

4.3 Effect of sliding distance

The effect of sliding distance on the wear rate of AA6061/ZrB_2 in-situ composite is depicted in Fig. 7. The figure shows that the wear rate increases linearly with the increase of sliding distance.

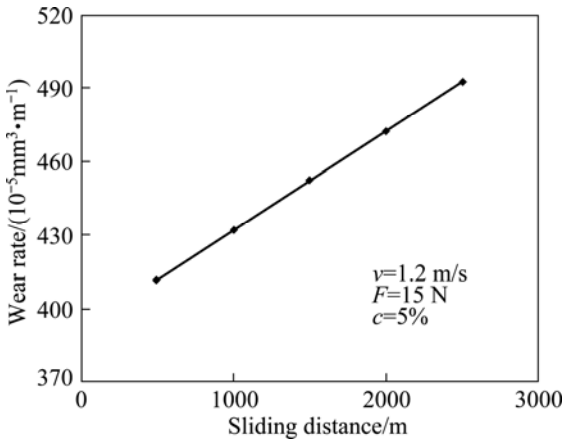

Fig. 7 Effect of sliding distance on wear rate

The asperity-to-asperity contact of the relatively moving counter surfaces initiates the proceedings of sliding wear. The asperities of the counter surface can be considered sharper and harder during initial wear stage. Those sharp asperities are subjected to higher amount of stress. The stress concentration on sharp asperities increases and in due course they deform plastically. Asperities having higher degree of sharpness are fractured due to normal and shear stress acting at the contact surface. A fraction of energy is spent on plastic deformation during sliding. The subsequent material removal requires higher energy to overcome the frictional force, which results in heating of the counter surfaces. The initial stage of wear consists of fragmentation of asperities and removal of material due to cutting of hard asperities into the softer pin surface. The frictional heat increases with increasing sliding distance. The temperature of the contact surface increases monotonically due to adiabatic heating. The increased degree of softening of pin surface owing to higher heat raises the rate of deformation. The generation of subsurface micro cracks leads to the removal of wear debris. As a result, the wear rate increases with the increase in sliding distance.

Figure 8 reveals the SEM micrographs of the wear surface of the fabricated composite at sliding distances of 500 m and 2500 m. In Fig. 8(a), fragmentation of asperities, wear debris and delamination of the matrix alloy are visible when the sliding distance is 500 m. The

grooves are apparently shallow and continuous. Fewer cracks are seen. In Fig. 8(b), deep grooves due to increased ploughing action are visible when the sliding distance is 2500 m. The size and propagation of cracks are more pronounced than those of the wear surface tested with a sliding distance of 500 m. The wear surface morphology indicates that it has been subjected to higher frictional heat. The increase in wear rate of the composite with increased sliding distance is evident from the wear surface of the composite.

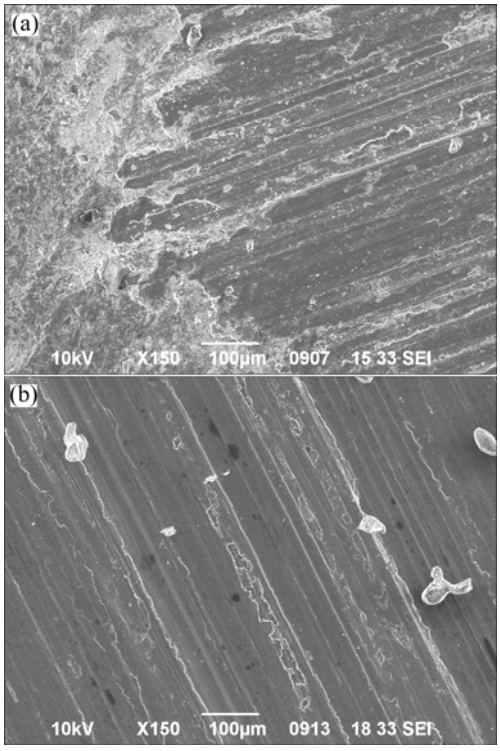

Fig. 8 SEM micrographs of wear surface of fabricated composite tested with sliding distance of 500 m (T19) (a) and 2500 m (T20) (b)

4.4 Effect of normal load

Figure 9 depicts the effect of normal load on the wear rate of AA6061/ZrB_2 in-situ composite. The figure shows that the wear rate increases linearly with the increase of normal load.

The obtained results are in good agreement with the well known Archard law of wear equation which states that the wear rate increases linearly with increasing the applied pressure [28]. The applied pressure increases when the normal load increases. Two counter surfaces involve in relative motion during sliding under normal load. Both the surfaces are not perfectly smooth and contain asperities in large number. The shape, height and sharpness of the asperities vary in the same material. During the initial period of sliding those asperities whose height is more than the critical value penetrate deeply into the softer surface of the pin and induce micro ploughing. The fracture, deformation and fragmentation

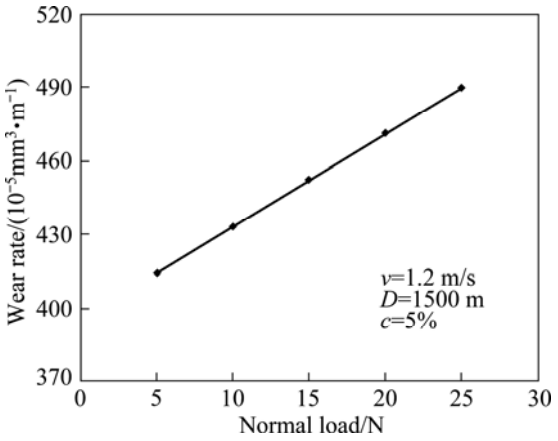

Fig. 9 Effect of normal load on wear rate

of asperities occur. As the normal load increases, the depth of penetration of hard asperities to the softer pin increases. A higher degree of material transfer between the counter surfaces takes place. The tendency to subsurface deformation and micro cracking increases with the increase in normal load. Particle fragmentation is another reason for the increased wear rate. The rate of fragmentation increases as the normal load increases. The normal load also influences the contact between the counter surfaces [29]. The degree of contact determines the degree of frictional heat generated. The contact becomes intimate with increased normal load and more frictional heat is accumulated at the interface, which results in softening of the pin surface. It becomes easier for the asperities in the counter surface to penetrate into the surface of the softened pin causing increased wear rate.

Figure 10 reveals the SEM micrographs of the wear surface of the fabricated composite at normal loads of 5 N and 25 N. In Fig. 10(a), the degree of development of cracks on the wear surface is not much at normal load of 5 N. Continuous wear grooves and some relatively smooth as well as damaged surfaces are seen. The wear surface exhibits micro ploughing of counter surface on the pin. Flaky shaped wear debris is formed as a result of propagation of cracks and fragmentation of asperities. The delamination of the matrix alloy is visible. In Fig. 10(b), the degree of formation of cracks on the wear surface is more at normal load of 25 N. The propagation of both longitudinal and transverse cracks is clearly visible. The grooves and cavities are deeper compared to the wear surface at normal load of 5 N. The cavities are formed due to delamination and tearing of surface materials. The deformation of subsurface is also seen. The appearance of the wear surface indicates that it has been subjected to higher frictional heat. It is evident from the wear surface that increase in normal load increases the wear rate of the composite.

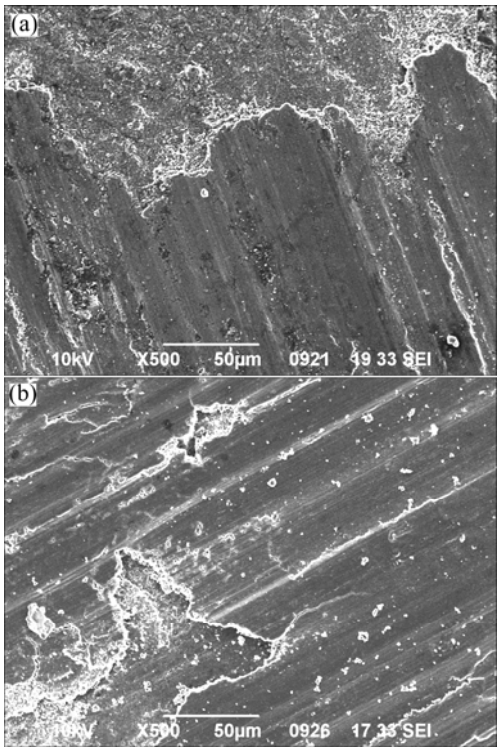

Fig. 10 SEM micrographs of wear surface of fabricated composite tested at normal load 5 N (T21) (a) and 25 N (T22) (b)

5 Conclusions

1) A mathematical model was developed to predict the wear rate of AA6061/(0−10%)ZrB_2 in-situ composites.

2) The in-situ formed ZrB_2 particles improve the wear resistance of the composite.

3) The dry sliding wear behavior of the composite is nonlinear.

4) The wear parameters of sliding velocity, sliding distance and normal load are inversely proportional to the wear resistance.

Acknowledgements

The authors are grateful to the Management and Department of Mechanical Engineering, Coimbatore Institute of Technology, Coimbatore, India for extending the facilities to carry out this investigation. The authors also acknowledge the financial support rendered by All India Council for Technical Education, Govt. of India. Authors are also thankful to Mr. S. J. Vijay, Mr. K. Kalaiselvan, Mr. B. Ashok Kumar, Mr. A. Raja, Mr. A. Samson Ratnakumar, Mr. S. Vijaya Ganesh, Mr. Palanisamy and Mr. Mahalingam for their assistance. The corresponding author acknowledges Department of Science and Technology, Govt. of India for providing INSPIRE fellowship.

References

[1] HEINZ A, HASZLER A, KEIDEL C, MOLDENHAUER S, BENEDICTUS R, MILLER W S. Recent development in aluminium alloys for aerospace applications [J]. Materials Science and Engineering A, 2000, 280: 102−107.

[2] MILLER W S, ZHUANG L, BOTTEMA J, WITTEBROOD A J, SMET P D, HASZLER A, VIEREGGE A. Recent development in aluminium alloys for the automotive industry [J]. Materials Science and Engineering A, 2000, 280: 37−49.

[3] MIRACLE D B. Metal matrix composites — From science to technological significance [J]. Composites Science and Technology, 2005, 65: 2526−2540.

[4] ROSSO M. Ceramic and metal matrix composites: Routes and properties [J]. Journal of Materials Processing Technology, 2006, 175: 364−375.

[5] SANNINO A P, RACK H J. Dry sliding wear of discontinuously reinforced aluminum composites: Review and discussion [J]. Wear, 1995, 189: 1−19.

[6] HASHIM J, LOONEY L, HASHMI M S J. The enhancement of wettability of SiC particles in cast aluminium matrix composites [J]. Journal of Materials Processing Technology, 2001, 119: 329−335.

[7] KENNEDY A R, WYATT S M. The effect of processing on the mechanical properties and interfacial strength of aluminium/TiC MMCs [J]. Composites Science and Technology, 2000, 60: 307−314.

[8] FOGAGNOLO J B, ROBERT M H, NAVAS E M R, TORRALBA J M. 6061 Al reinforced with zirconium diboride particles processed by conventional powder metallurgy and mechanical alloying [J]. Journal of Materials Science, 2004, 39: 127−132.

[9] RAJAN T P D, PILLAI R M, PAI B C, SATYANARAYANA K G, ROHATGI P K. Fabrication and characterisation of Al–7Si–0.35Mg/fly ash metal matrix composites processed by different stir casting routes [J]. Composites Science and Technology, 2007, 67: 3369−3377.

[10] TJONG S C, MA Z Y. Microstructural and mechanical characteristics of in situ metal matrix composites [J]. Materials Science and Engineering R, 2000, 29: 49−113.

[11] SONBER J K, MURTHY T S R C, SUBRAMANIAN C, KUMAR S, FOTEDAR R K, SURI A K. Investigations on synthesis of ZrB_2 and development of new composites with HfB_2 and $TiSi_2$ [J]. International Journal of Refractory Metals and Hard Materials, 2011, 29: 21–30.

[12] GUO S Q, KAGAWA Y, NISHIMURA T. Mechanical behavior of two-step hot-pressed ZrB_2-based composites with $ZrSi_2$ [J]. Journal of the European Ceramic Society, 2009, 29: 787–794.

[13] MANDAL A, CHAKRABORTY M, MURTY B S. Effect of TiB_2 particles on sliding wear behaviour of Al–4Cu alloy [J]. Wear, 2007, 262: 160–166.

[14] KUMAR S, CHAKRABORTY M, SARMA V S, MURTY B S. Tensile and wear behaviour of in situ Al–7Si/TiB_2 particulate composites [J]. Wear, 2008, 265: 134–142.

[15] HERBERT M A, MAITIB R, MITRA R, CHAKRABORTY M. Wear behaviour of cast and mushy state rolled Al–4.5Cu alloy and in-situ Al4.5Cu–5TiB_2 composite [J]. Wear, 2008, 265: 1606–1618.

[16] ZHANG S L, ZHAO Y T, CHEN G, CHENG X N, HUO X Y. Fabrication and dry sliding wear behavior of in situ Al–K_2ZrF_6–KBF_4 composites reinforced by Al_3Zr and ZrB_2 particles [J]. Journal of Alloys and Compounds, 2008, 450: 185−192.

[17] KUMAR G N, NARAYANASAMY R, NATARAJAN S, BABU S P K, SIVAPRASAD K, SIVASANKARAN S. Dry sliding wear behavior of AA 6351-ZrB_2 in situ composite at room temperature [J]. Materials and Design, 2010, 31: 1526–1532.

[18] KARTHIKEYAN R, BALASUBRAMANIAN V. Predictions of the optimized friction stir spot welding process parameters for joining AA2024 aluminum alloy using RSM [J]. International Journal of Advanced Manufacturing Technology, 2010, 51: 173–183.

[19] THAMBIDURAI M, MUTHUKUMARASAMY N, MURUGAN N, AGILAN S, VASANTHA S, BALASUNDARAPRABHU R. Development of mathematical model for prediction and optimization of particle size in nanocrystalline CdS thin films prepared by sol-gel spin-coating method [J]. Metallurgical and Materials Transactions B, 2010, 41: 1338−1345.

[20] KUMAR S, BALASUBRAMANIAN V. Effect of reinforcement size and volume fraction on the abrasive wear behaviour of AA7075Al/SiC_p P/M composites—A statistical analysis [J]. Tribology International, 2010, 43: 414–422.

[21] RAJAKUMAR S, MURALIDHARAN C, BALASUBRAMANIAN V. Predicting tensile strength, hardness and corrosion rate of friction stir welded AA6061-T6 aluminium alloy joints [J]. Materials and Design, 2011, 32: 2878−2890.

[22] GOPALAKRISHNAN S, MURUGAN N. Prediction of tensile strength of friction stir welded aluminum matrix TiC_p particulate reinforced composite [J]. Materials and Design, 2011, 32: 462−467.

[23] RAJAKUMAR S, MURALIDHARAN C, BALASUBRAMANIAN V. Establishing empirical relationships to predict grain size and tensile strength of friction stir welded AA 6061-T6 aluminium alloy joints [J]. Transactions of Nonferrous Metal Society of China, 2010, 20: 1863−1872.

[24] DINAHARAN I, MURUGAN N, PARAMESWARAN S. Influence of in-situ formed ZrB_2 particles on microstructure and mechanical properties of AA6061 metal matrix composites [J]. Materials Science and Engineering A, 2011, 528: 5733−5740.

[25] BERAHA E, SHPIGLER B. Color metallography [M]. Ohio: American Society for Metals, 1977.

[26] MONTGOMERY D G. Design and analysis of experiments [M]. Hoboken: John Wiley & Sons, 2009.

[27] RAO R N, DAS S. Effect of SiC content and sliding speed on the wear behaviour of aluminium matrix composites [J]. Materials and Design, 2011, 32: 1066−1071.

[28] ARCHARD J F. Contact and rubbing of flat surfaces [J]. Journal of Applied Physics, 1953, 24: 981−988.

[29] RAO R N, DAS S. Effect of applied pressure on the tribological behaviour of SiC_p reinforced AA2024 alloy [J]. Tribology International, 2011, 44: 454−462.

AA6061/ZrB_2原位复合材料的干滑动磨损行为

I. DINAHARAN[1], N. MURUGAN[2]

1. Department of Mechanical Engineering, Karunya University, Coimbatore−641 114, Tamil Nadu, India;
2. Department of Mechanical Engineering, Coimbatore Institute of Technology, Coimbatore−641 014, Tamil Nadu, India

摘　要：通过往铝熔体中添加 K_2ZrF_6 和 KBF_4 制备 AA6061/ZrB_2 原位复合材料，并对该复合材料的干滑动磨损形为进行研究。构建了一数学模型来预测该复合材料的磨损速率。采用 4 因素 5 水平的中心复合旋转设计方法来减少实验工作量。考察滑动速度、滑动距离、载荷和 ZrB_2 质量分数这 4 个因素对制备的复合材料的磨损速率的影响，通过观察磨损表面形貌分析这些因素的影响。结果表明，原位生成的 ZrB_2 颗粒改善了复合材料的磨损性能。该复合材料的磨损速率随着滑动速度、滑动距离和载荷的增加而增加。

关键词：铝基复合材料；硼化锆；干滑动磨损；数学模型

(Edited by YUAN Sai-qian)